

# Rational Design of Novel Allosteric Dihydrofolate Reductase Inhibitors Showing Antibacterial Effects on Drug-Resistant *Escherichia coli* Escape Variants

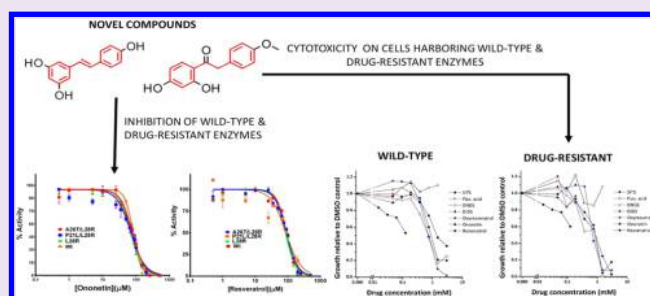
Bharath Srinivasan,<sup>†</sup> João V. Rodrigues,<sup>‡</sup> Sam Tonddast-Navaei,<sup>†</sup> Eugene Shakhnovich,<sup>‡</sup> and Jeffrey Skolnick<sup>\*,†</sup>

<sup>†</sup>Center for the Study of Systems Biology, School of Biology, Georgia Institute of Technology, 950 Atlantic Drive, Atlanta, Georgia 30332, United States

<sup>‡</sup>Department of Chemistry and Chemical Biology, Harvard University, 12 Oxford Street, Cambridge, Massachusetts 02138, United States

## Supporting Information

**ABSTRACT:** In drug discovery, systematic variations of substituents on a common scaffold and bioisosteric replacements are often used to generate diversity and obtain molecules with better biological effects. However, this could saturate the small-molecule diversity pool resulting in drug resistance. On the other hand, conventional drug discovery relies on targeting known pockets on protein surfaces leading to drug resistance by mutations of critical pocket residues. Here, we present a two-pronged strategy of designing novel drugs that target unique pockets on a protein's surface to overcome the above problems. Dihydrofolate reductase, DHFR, is a critical enzyme involved in thymidine and purine nucleotide biosynthesis. Several classes of compounds that are structural analogues of the substrate dihydrofolate have been explored for their antifolate activity. Here, we describe 10 novel small-molecule inhibitors of *Escherichia coli* DHFR, *Ec*DHFR, belonging to the stilbenoid, deoxybenzoin, and chalcone family of compounds discovered by a combination of pocket-based virtual ligand screening and systematic scaffold hopping. These inhibitors show a unique uncompetitive or noncompetitive inhibition mechanism, distinct from those reported for all known inhibitors of DHFR, indicative of binding to a unique pocket distinct from either substrate or cofactor-binding pockets. Furthermore, we demonstrate that rescue mutants of *Ec*DHFR, with reduced affinity to all known classes of DHFR inhibitors, are inhibited at the same concentration as the wild-type. These compounds also exhibit antibacterial activity against *E. coli* harboring the drug-resistant variant of DHFR. This discovery is the first report on a novel class of inhibitors targeting a unique pocket on *Ec*DHFR.



Traditional drug-discovery initiatives have targeted pockets, predominantly active sites and in a few cases allosteric sites, on a protein's surface.<sup>1</sup> The problem with this approach is the widespread occurrence of undesirable, and occasionally lethal, side effects shown by a majority of drugs due to off-target interactions apart from the rapid acquisition of drug resistance against these molecules due to mutations on the protein. It has been recently demonstrated that drug cross-reactivity may be a direct consequence of the remarkably small number of geometrically distinct pockets.<sup>2,3</sup> Incremental changes in the metabolites have failed to rescue this problem given the high conservation of interaction profiles that govern ligand–protein interactions. This requires a new approach to designing drugs that can circumvent the limitations of targeting conventional protein pockets by using a series of ligands with incremental modifications.

Dihydrofolate reductase, DHFR, is an important enzyme in the *de novo* pathway of purine and thymidine synthesis.<sup>4</sup> Small

molecules targeting this enzyme have been shown to possess utility as potential antibiotics<sup>4</sup> and anticancer agents.<sup>5</sup> However, this enzyme develops rapid resistance to available antifolates by acquiring mutations on residues critical for binding. It has been demonstrated that clinical levels of resistance to known antifolates can be obtained after merely three rounds of directed-evolution efforts.<sup>6</sup> Further, attempts at understanding the evolutionary paths for development of antibiotic resistance in DHFR led to the understanding that resistance evolves by sequential fixation of mutations through ordered pathways. The most prominent mutants conferring trimethoprim resistance were either on the promoter (−9G → A; −35C → T) or on the DHFR protein (P21, A26, L28R, W30, and I94) and their combinations.<sup>7</sup> Furthermore, physical–chemical studies on

Received: February 26, 2017

Accepted: May 19, 2017

Published: May 19, 2017



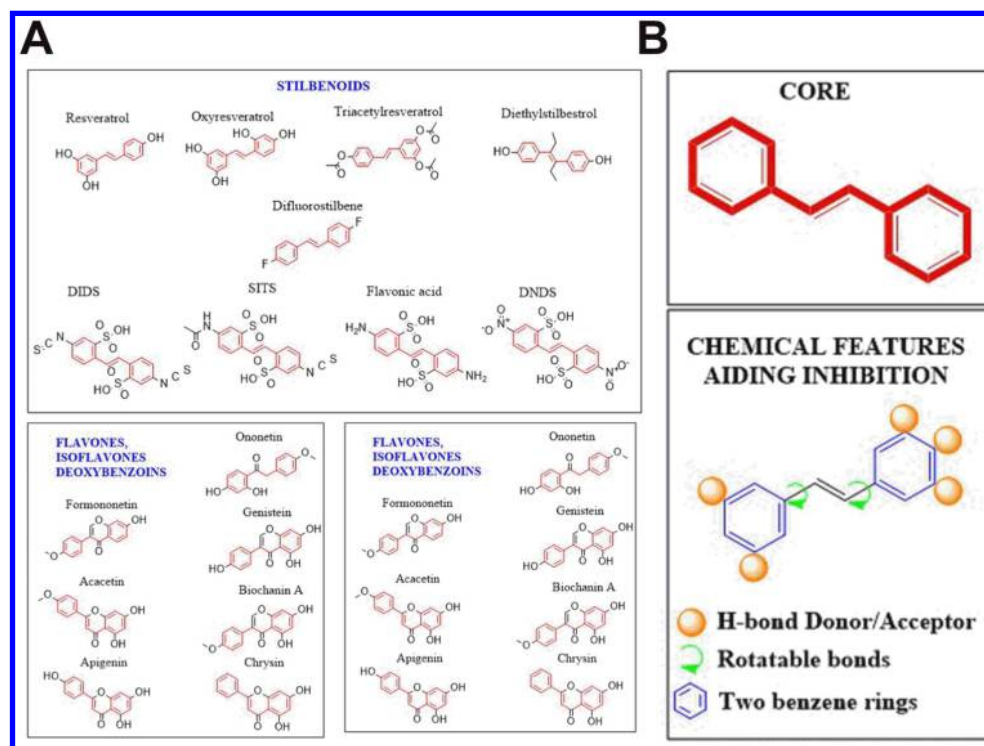


**Figure 1.** Structures and molecular-features governing *EcDHFR* inhibition. (A) Structures of various small molecules employed in this study classified based on the parental scaffold. (B) Minimal molecular features that determine the inhibition potential of a small molecule for *EcDHFR*. The number and positioning of hydrogen bonding donors/acceptors on the benzene ring is representative and can vary depending on the potency of the inhibition (See Table 1).

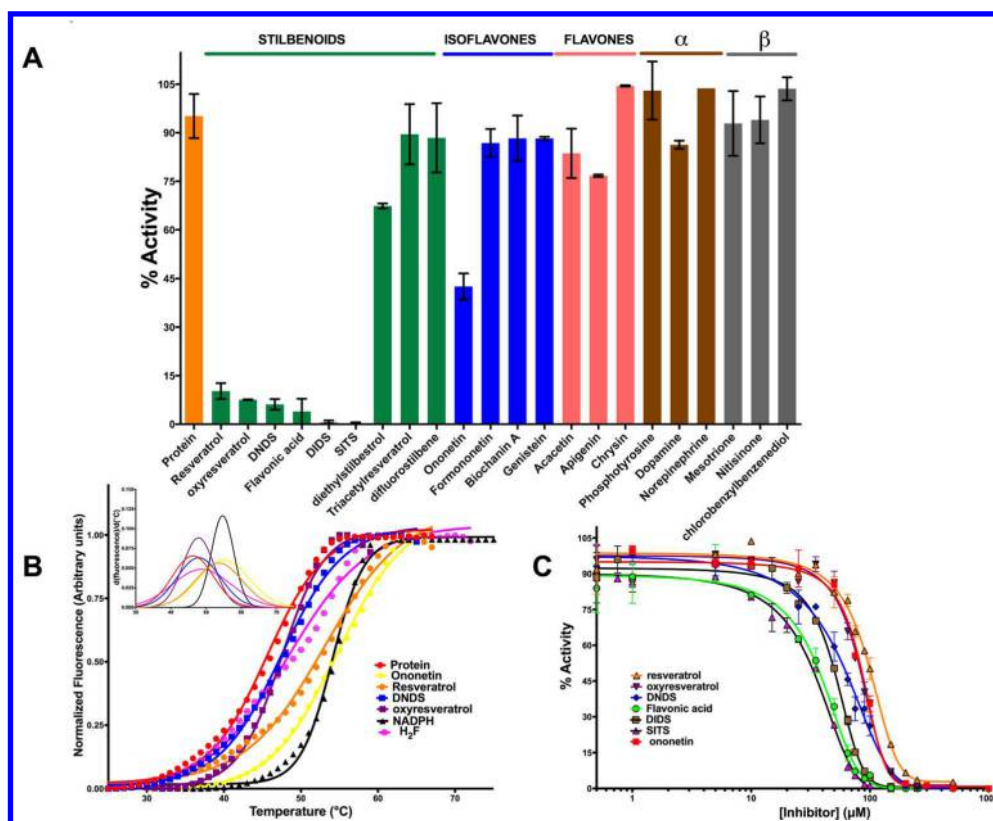


**Figure 2.** Binding and inhibition of *EcDHFR* by small molecules. (A) Single-concentration assessment of enzyme inhibition by small molecules. Each histogram represents the activity in the presence of 1 mM inhibitor. (B) DSF curves for small molecules showing inhibition. The inhibitors were kept fixed at 100 μM. (C) IC<sub>50</sub> determination for deoxybenzoins, stilbene, and chalcone analogues for *EcDHFR*.

these mutants have demonstrated that the decreased affinity to the drug comes at the cost of catalytic efficiency and protein stability.<sup>8</sup> To address the issue of rapid drug-resistance acquisition, several classes of compounds have been explored for their potential antifolate activity.

Analogues of the cofactor NADPH have been reported as potential inhibitors of *Ec*DHFR.<sup>9</sup> However, NADPH analogues would not be ideal candidates as clinically relevant inhibitors because of the extensive cross-reactivity that would arise due to possible targeting of NADPH binding sites in diverse enzymes and the extensive presence of nucleotide-binding pockets on several different proteins.

Most reported inhibitors for DHFRs are structural analogues of its substrate dihydrofolate and act by competitively displacing the latter. Antifolates available as inhibitors of DHFRs contain the 2,4-diamino-1,3-diazapharmacophore.<sup>10</sup> Predominant classes of dihydrofolate analogues employed as inhibitors include diaminoquinazoline,<sup>11–16</sup> diaminopyrimidine,<sup>17–20</sup> diaminopteridine,<sup>21</sup> and diaminotriazines.<sup>22,23</sup> However, it should be noted that the development of rapid drug resistance to antifolate antibiotics belonging to any of the above-mentioned classes poses an immense challenge.<sup>24</sup>

This necessitates discovering novel scaffolds that not only can overcome the excessive reliance on folate analogs but also should inhibit the enzyme by binding to unique sites on the enzyme. In a previous study employing our novel pocket-based VLS tool *PoLi*, we identified ononetin as a unique scaffold binding to *Ec*DHFR.<sup>25</sup> The current study explores detailed inhibition kinetics to demonstrate that ononetin is a novel inhibitor of *Ec*DHFR showing a unique mechanism of inhibition. Further, using the principles of scaffold hopping and structure–activity relationship (SAR), we discovered 10 novel small-molecule inhibitors of *Ec*DHFR. These inhibitors have a novel scaffold distinct from either the substrate or cofactor of *Ec*DHFR and target a unique pocket on the protein. Most importantly, this study demonstrates that these inhibitors are capable of inhibiting rescue variants that show reduced affinity for most available antifolates and show cytotoxic effect against *E. coli* that harbor these DHFR variants.

## RESULTS AND DISCUSSIONS

**Scaffold Hopping and SAR To Assess the Molecular Features Governing *Ec*DHFR Inhibition.** The VLS algorithm, *PoLi*, predicted ononetin as potential binder of *Ec*DHFR.<sup>25</sup> Consistent with VLS predictions, the small molecule showed binding to *Ec*DHFR as assessed by differential scanning fluorimetry (DSF).<sup>25</sup> To understand whether the demonstrated binding by ononetin translates into inhibition, we assessed its inhibitory effect on *Ec*DHFR activity. Inhibition studies indicate that ononetin inhibits the enzyme (Figure 2).

To validate the above observation and tease apart the molecular features that might be contributing to binding and inhibition, a systematic SAR and knowledge-based scaffold hopping was employed. This led to the screening of 22 molecules belonging to the deoxybenzoin, isoflavones, flavones, stilbenoids, catecholamine derivatives, and HPPD inhibitors (Figure 1 A). Figure 2 A summarizes the results from the inhibition assessment study. No binding to or inhibition of *Ec*DHFR activity was detected for either isoflavones or flavones. Furthermore, if the number of degrees of freedom in the bonds connecting the two benzenes is less than 3, no significant inhibition is observed. Lack of a benzene ring or substitution of

a cyclohexane instead of a benzene also led to abolishment of inhibition. Furthermore, substitutions on the benzene ring that are not capable of either accepting or donating hydrogen bonds also abolished inhibition of the enzyme. These observations point out that the presence of two benzene rings, a linker with a minimum of three degrees of freedom, and presence of hydrogen bonding donors or acceptors on the benzene rings constitute the essential molecular features that determine whether a molecule will inhibit *Ec*DHFR (Figure 1 B).

Six stilbenoid compounds, namely, resveratrol, oxyresveratrol, SITS, DIDS, flavonic acid, and DNDS, showed inhibition in the initial screen apart from that observed with ononetin. At 100  $\mu$ M concentration, the inhibition by stilbenoids was more pronounced than that shown by ononetin (Figure 2 A). Subsequently, detailed binding (Figure 2 B) and concentration dependence of inhibition for the various small molecules was assessed (Table 1 and Figure 2 C).

**Table 1. Inhibition and Binding Parameters for the Various Small Molecules**

S. No.	compound	IC <sub>50</sub> ( $\mu$ M)	K <sub>app</sub> ( $\mu$ M) <sup>b</sup>	$\Delta T_m$ ( $^{\circ}$ C) <sup>c</sup>
1	SITS	32.3 $\pm$ 1.8	32.3	<i>d</i>
2	flavonic acid	36.7 $\pm$ 3.1	36.7	<i>d</i>
3	DNDS <sup>a</sup>	45.3 $\pm$ 10.1	45.3	1.9
4	DIDS	51.0 $\pm$ 1.7	51.0	<i>d</i>
5	oxyresveratrol	81.8 $\pm$ 1.8	81.8	1.9
6	resveratrol	95.7 $\pm$ 3.0	95.7	8.3
7	ononetin	83.4 $\pm$ 1.1	83.4	3.2

<sup>a</sup>Dinitro disulfonic acid. <sup>b</sup>Calculated theoretically with the assumption that it is noncompetitive inhibition, that is,  $K_i = IC_{50}$  when  $S = K_m$  or  $S \gg K_m$  or  $S \ll K_m$ . <sup>c</sup>All the thermal shifts were done at a single concentration of 0.5 mM small molecule. <sup>d</sup>No signal possibly due to interference with the extrinsic fluorophore dye.

As an additional step, we tested ten compounds from the chalcones family, with an additional linker bond that connects the two benzenes, for their potential in inhibiting *Ec*DHFR. Scaffold hopping (Figure S1A) and preliminary SAR (Figure S1B) was carried out for these chalcones. Three of the assessed compounds, with hydrogen bonding donors or acceptors on the benzene ring, showed unequivocal inhibition (Figure S1 B). This shows that any compound possessing 3–4 degrees of freedom connecting the two benzene moieties, with appropriate hydrogen bonding acceptors or donors, can inhibit *Ec*DHFR.

To rule out nonspecific protein-aggregation-induced inhibition, two hits belonging to the deoxybenzoin and stilbene families were assessed for potentially causing aggregation of the protein. Experiments were performed with dynamic light scattering at 100  $\mu$ M protein. Results indicate that there is no small-molecule-mediated aggregation of the protein sample, clearly showing that the inhibition is highly specific (Figure S2).

**Detailed Kinetic Characterization of Inhibition.** *Ononetin as an Uncompetitive Inhibitor of H<sub>2</sub>F Binding.* To further understand the nature of the inhibition shown by the deoxybenzoin ononetin vis-à-vis H<sub>2</sub>F, we resorted to detailed inhibition kinetics. Dihydrofolate was titrated at several fixed concentrations of ononetin and at saturating NADPH. The resulting curves from the experiment were globally fit to models for various types of inhibition. A sum-of-square F-test was performed to validate the nonlinear fits. The experimental curves showed the best fit to the model for uncompetitive

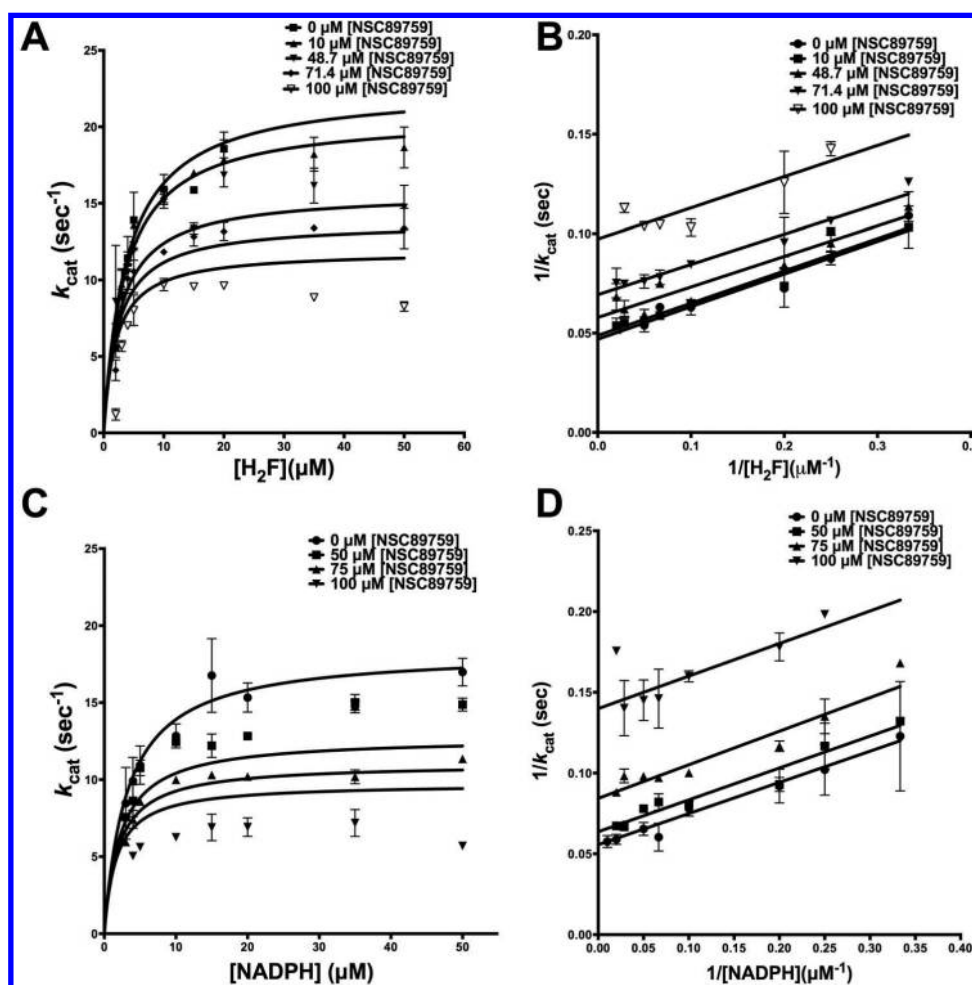


**Figure 3.** Typical inhibition kinetics of *EcDHFR* by ononetin at low substrate/inhibitor concentrations. (A) Competition experiments of ononetin against  $\text{H}_2\text{F}$  at saturating NADPH. (B) Lineweaver–Burk plot of the data from panel A. (C) Competition experiments of ononetin against NADPH at saturating concentration of  $\text{H}_2\text{F}$ . (D) Lineweaver–Burk plot of the data from panel C.

**Table 2. Inhibition Parameters and Mechanism of the Small Molecule Ononetin for *EcDHFR* at Different Substrate and Cofactor Concentrations**

inhibitor	substrate	lower substrate <sup>a</sup>		higher substrate
		inhibition mechanism	$\alpha K_i$ ( $\mu\text{M}$ )	$K_i$ ( $\mu\text{M}$ ) <sup>b</sup>
ononetin	$\text{H}_2\text{F}$	uncompetitive	$111.2 \pm 12.37$	$22.15 \pm 10.94$
	NADPH	uncompetitive	$113.2 \pm 13.1$	$72.69 \pm 22.18$
resveratrol	$\text{H}_2\text{F}$	linear mixed-type	$88.30 \pm 6.02$	$31.48 \pm 8.85$
SITS	$\text{H}_2\text{F}$	noncompetitive	$39.63 \pm 3.01$	$35.86 \pm 11.23$
flavonic acid	$\text{H}_2\text{F}$	noncompetitive	$76.25 \pm 6.82$	$18.32 \pm 9.68$

<sup>a</sup>The reported values are for the global nonlinear fits. <sup>b</sup>Values from fit to equation for substrate inhibition at highest inhibitor concentration. Note that the values reported here are not from global nonlinear fits and differ from one inhibitor to another depending on the highest concentration employed for the respective inhibitor (Figure S5).

inhibition ( $R^2 = 0.84$ ) (Figure 3A) giving a value for  $\alpha K_i$ , the equilibrium dissociation constant for the uncompetitive inhibitor, of  $111.2 \pm 12.37 \mu\text{M}$  (Table 2). For ease of visualization, the data were transformed and plotted as double-reciprocal Lineweaver–Burk plot, LB. Figure 3B shows parallel lines on the LB-plot, which is further indicative of uncompetitive displacement of substrate dihydrofolate by ononetin. This suggests an ordered binding event whereby  $\text{H}_2\text{F}$  binding facilitates inhibitor binding. This is a very unique observation that, to the best of our knowledge, has not been seen with any other DHFR-inhibitors. As has been pointed out

in the introduction, most known inhibitors of DHFR are analogues of  $\text{H}_2\text{F}$  and competitively displace the latter. In contrast, the experimental results suggest that an additional binding site is created upon  $\text{H}_2\text{F}$  binding that can accommodate the inhibitor ononetin.

In uncompetitive inhibition, the inhibitor usually binds reversibly to the ES complex yielding an inactive ESI complex. Hence  $V_{\text{max}}$  in the presence of the inhibitor will be lower than in its absence. However, the apparent  $K_m$  of the substrate also decreases indicating an affinity increase. The increase results from the reaction  $\text{ES} + \text{I} \rightarrow \text{ESI}$  that uses up some ES

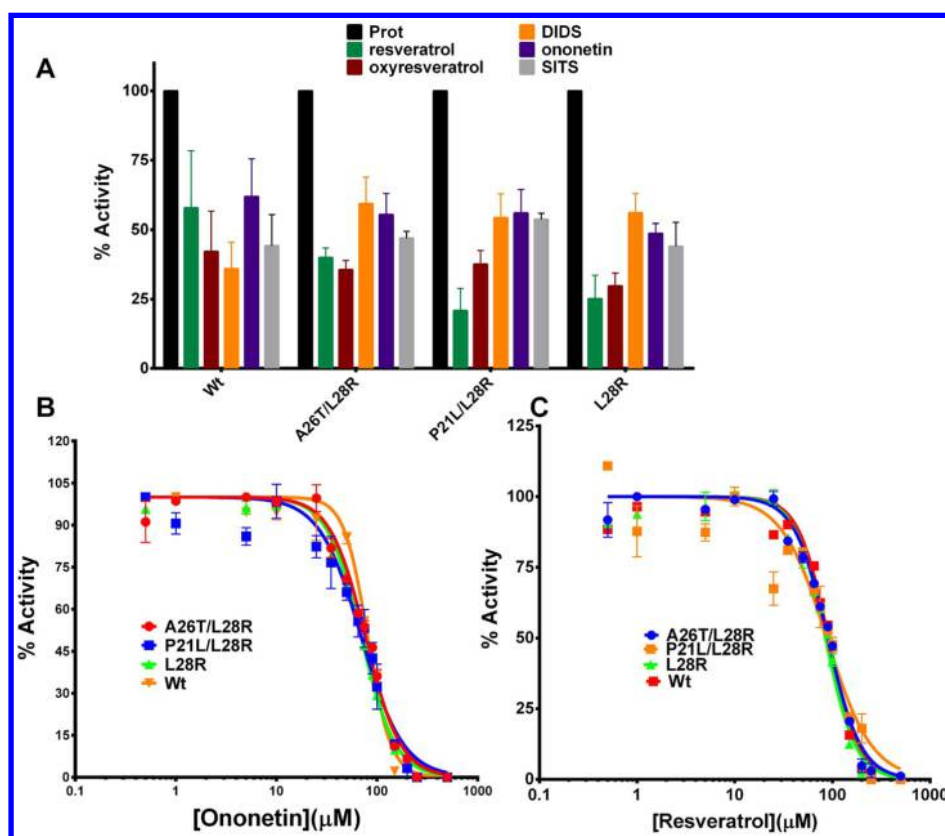


**Figure 4.** Assessment of inhibition for *EcDHFR* wild-type and rescue variants (A) by the deoxybenzoin and stilbenoid classes of small molecules. The assessment was carried out in duplicate at a single concentration of the inhibitor around its experimental  $IC_{50}$  values for the wild-type enzyme. (B) Estimation of  $IC_{50}$  values of ononetin for wild-type, A26T/L28R mutant, P21L/L28R mutant, and L28R mutants. (C) Estimation of  $IC_{50}$  values of resveratrol for wild-type, A26T/L28R mutant, P21L/L28R mutant, and L28R mutants.

causing the substrate-binding reaction  $E + S$  giving  $ES$  to proceed further to the right. However, this increased affinity is misleading and essentially represents a locked enzyme that can no longer turnover the substrate and does not indicate inhibitor-mediated substrate binding. In this case, the binding affinities for the inhibitor and the substrate are an order of magnitude different. While for the substrate dihydrofolate it is in lower micromolar range, for the inhibitor, the  $K_i$  is almost 0.1 mM. Hence, though the effect of substrate binding on inhibitor binding is pronounced, the reverse is not true. Hence, it can be stated with reasonable confidence that substrate binding facilitates inhibitor binding.

**Ononetin as Uncompetitive Inhibitor of NADPH Binding.** Inhibition of the cofactor NADPH binding by ononetin was also assessed. The experimental curves, once again, showed the best fit to the uncompetitive inhibition model (Figure 3C) yielding an  $\alpha K_i$  value of  $113.2 \pm 13.1 \mu\text{M}$ . As above, the LB plots showed parallel lines further indicative of uncompetitive inhibition (Figure 3D) and an ordered binding event whereby NADPH binding facilitates inhibitor binding. Further, this data is in agreement with reported mechanisms of DHFR inhibition by folate analogs.<sup>16,23</sup> It has been demonstrated that the binding of and inhibition by folate-analogs is conditional to NADPH binding.<sup>16,23</sup>

**Substrate Inhibition-like Behavior at High Substrate and Ononetin Concentrations.** Careful inspection of the nonlinear plots in Figure 3A,C shows pronounced nonlinearity at saturating substrate and high inhibitor concentrations. However, as has been demonstrated in previous studies<sup>16,23</sup> and by

inspection of curves at low inhibitor concentrations in Figure 3A,C shows, no substrate inhibition is seen in the absence of the inhibitor. This led us to hypothesize that the observed behavior might be indicative of a unique two-site binding inhibition mechanism displayed by ononetin.

To confirm this hypothesis, the experiment shown in Figure 3A,C was extended to high substrate and cofactor concentrations. As seen in Figure S3A,C, the resulting curves show pronounced substrate-inhibition-like behavior at higher inhibitor concentration. Further, fitting the curves to equations of substrate inhibition gave  $K_i$  values that kept decreasing (i.e., increasing potency of inhibition) with increasing substrate concentration indicative of substrate-inhibition like behavior by ononetin (Figure S3A,C). This pattern is clearly evident in the nonlinear LB plot (Figure S3B,D). This is a unique kinetic behavior displayed by this inhibitor and is the first of this kind to be observed with any reported *EcDHFR* inhibitors. Taken together, these patterns are likely indicative of either substrate–inhibitor, cofactor–inhibitor, or substrate–cofactor–inhibitor complex as the true inhibitor or an alternate site of binding for the inhibitor.

In summary, uncompetitive inhibition by the inhibitor at low substrate and cofactor concentrations and substrate inhibition-like behavior at high substrate and cofactor concentrations indicates that the kinetic model for inhibition may be more complex than preliminary analysis of the data suggests. Further, numerical analysis of data by fitting it to global models with multiple unknown variables would likely lead to overfitting.

In order to understand whether either the substrate or cofactor molecule forms a complex with ononetin, wavelength scans on UV-vis spectrophotometer were carried out with the individual metabolites and their combinations thereof. In summary, though no convincing evidence for complex formation between the substrate or cofactor and ononetin was seen, H<sub>2</sub>F and ononetin showed a spectrum that was markedly different than the spectrum of either H<sub>2</sub>F or ononetin alone (Figure S4). This was markedly different than the case of NADPH and ononetin where the composite spectrum was an additive equivalent of the two individual spectra (Figure S4).

It has to be once again reiterated here that these compounds are the first to show inhibition that is not competitive either against the cofactor or the substrate.

**Inhibition Mechanism Shown by Stilbenoid Inhibitors.** We performed detailed inhibition kinetics with a few representative stilbenoid compounds to understand whether they too show these unique mechanisms of inhibition that are not competitive against H<sub>2</sub>F. Substrate dihydrofolate was titrated at several fixed concentrations of resveratrol, flavonic acid, and SITS and at saturating NADPH. Figure S5 shows the global experimental points and the nonlinear fits of the experiments to the respective inhibition models for points that do not show substrate inhibition like behavior. The plots show fits either to noncompetitive or mixed-type inhibition indicating, once again, a distinct site of binding. Data for resveratrol fits well to the model for mixed-type inhibition, while data for SITS and flavonic acid fit the noncompetitive inhibition model better than equivalent models (Figure S5A–C). At high substrate and inhibitor concentrations, the curve starts resembling substrate inhibition like behavior as seen with ononetin, possibly indicative of two-site binding.

**Novel Class of Inhibitors Targeting Drug-Resistant EcDHFR Variants.** Often, protein targets develop resistance against a small-molecule drug by acquiring mutations that either function to weaken the binding or decrease the potency of inhibition of the small molecule.<sup>7</sup> Such mutations come at an evolutionary cost vis-à-vis enzyme stability and catalytic-turnover ability.<sup>8</sup> Previous work on the laboratory evolution of resistance of *E. coli* against trimethoprim demonstrated that the resistance is acquired through exclusive mutations in the gene encoding DHFR. We wanted to test whether a subset of the newly discovered small-molecule inhibitors could inhibit the drug-resistant variants of the EcDHFR. With this intention, drug-resistant single (L28R) and double mutants (A26T/L28R and P21L/L28R) were expressed and purified to homogeneity. Before assessing the new molecules, classical and slow-onset tight binding inhibitors that are structural analogues of substrate dihydrofolate reported by us in our previous studies were assessed.<sup>11,15,16,23</sup> The small molecules belonged to the diaminotriazine, diaminopyrroloquinazoline, and diaminopteridine class of molecules. The molecules were assessed at their respective IC<sub>50</sub> values in duplicate against the wild-type, one single mutant, and two double mutants. As can be seen from Figure S6, though all the molecules inhibit the wild-type enzyme by ~50-fold as is expected, they fail to inhibit the mutant enzymes. However, molecules belonging to deoxybenzoin and stilbenoid families inhibited both the wild-type enzyme and the drug-resistant mutants (Figure 4A). We would like to point out that these are the first set of molecules that inhibit these drug-resistant variants of EcDHFR and have the potential to be developed into next generation antibiotics against such rescue variants of the opportunistic pathogen.

Point estimation of inhibition could sometimes be misleading. Hence, for two promising hits, ononetin and resveratrol, IC<sub>50</sub> values were estimated for the wild-type and the three mutant variants. For both ononetin (Figure 4B) and resveratrol (Figure 4C), the IC<sub>50</sub> curves are superimposable indicating that these new classes of molecules have equal potency in inhibiting both the drug-resistant mutant variants and the wild-type enzyme. It should be pointed out that the drug-resistance-conferring mutations are localized either in or proximal to the substrate-binding pocket. These small molecules inhibiting the mutants as potently as the wild-type indirectly vindicates our conclusions from the kinetic studies showing a distinct site of binding different from the substrate-binding site. Any overlap of binding site with the mutation-harboring region would be expected to perturb the binding, and thus inhibition, either favorably or unfavorably as was seen with diaminotriazine, diaminopyrroloquinazoline, and diaminopteridine group of compounds.

**Binding-Site Prediction and Potential Mechanism of Inhibition.** In addition to the large catalytic pocket comprised of the NADP- and folate-binding sites, CAVITATOR detected three additional pockets (Table S2). These new pockets are much smaller than the catalytic-pockets in terms of both volume and number of amino-acids. The main catalytic site has more than 40 amino acids and a volume greater than 1000 Å<sup>3</sup>, whereas the new pockets have 12–15 amino acids and volumes of approximately 150–300 Å<sup>3</sup>. Figure S7 shows the location of these predicted pockets with respect to the catalytic site. Though being adjacent to the catalytic site, these pockets do not share any amino acids with the former. PKT2 is the largest of all three new pockets located below the catalytic site as shown in Figure S7A. It is a shallow pocket comprised mostly of loops that are wrapped around the β-sheets (Figure S7B) below the Met-20 loop. PKT3 is located close to the folate-binding site (Figure S7C) in a cleft between a helix and a β-sheet behind the folate-binding site. PKT4, on the other hand, is formed by the space between two short helices (Figure S7D) located behind the binding site of the adenine moiety of NADP.

Next, we compared these new pockets with the available holo-pockets. Interestingly, PKT4 has significant similarity (statistical *p*-value of  $0.89 \times 10^{-4}$ ) with the bromo-resveratrol binding site of human Sirt3<sup>26</sup> (PDB ID 4C78). In human Sirt3, bromo-resveratrol is in contact with six amino acids, among which five residues get perfectly aligned (two out of five are identical amino-acids) with amino acids in PKT4 (Table S3 and Figure 5). According to the interactions between bromo-resveratrol and Sirt3 calculated by PoseView<sup>27</sup> and reported on the corresponding PDB page, the carbonyl group of Met-311's backbone is responsible for hydrogen bonding with the bromo-resveratrol. In our pocket alignment, Met-311 of Sirt3 is aligned with Lys-106 of DHFR with a C<sub>α</sub>–C<sub>α</sub> distance of 0.171 Å. This perfect alignment of the hydrogen-bond acceptor carbonyl groups, together with the alignment of the neighboring amino acids (Figure 5), suggests that the pocket can accommodate resveratrol-like molecules. In addition to their pocket similarity, we would like to emphasize that both PKT4 in DHFR and bromo-resveratrol binding site in Sirt3 are located in a Rossmann-fold and there is weak global similarity (TM-Score = 0.42) between DHFR and Sirt3.

Figure S8 shows the structure of NADP-bound DHFR and bromo-resveratrol copied from Sirt3 using their pocket alignment. Amino acids inside PKT4 are adjacent to the

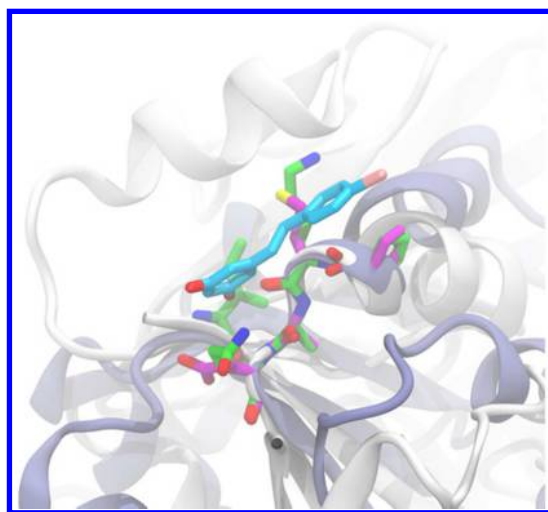


**Figure 5.** Superposition of *EcDHFR* (white) and its aligned pocket residues (green) onto the best template (ice blue), PDB ID 4C78, and its pocket residues (magenta) binding bromo-resveratrol (turquoise).

amino acids (Leu-62, Val-78, Gln102) that are in contact with the adenine moiety of NADP. One possible explanation for the mechanism of inhibition by resveratrol-like molecules could be perturbations in the adenine-binding site of NADP because of inhibitor binding at PKT4. However, this needs to be further investigated.

**Inhibition of *E. coli* Growth Encoding Wild-type vs Mutant Variants of DHFR.** Subsequent to obtaining the above-mentioned results, we tested the activity of a subset of small molecules targeting DHFR as bacterial growth inhibitors using *E. coli* cells. In addition, we also tested the *E. coli* mutant strain in which the chromosomal DHFR-coding gene *folA* was replaced by a drug-resistant variant (L28R) known to increase resistance to trimethoprim approximately 50-fold.<sup>8,28</sup> The drug dose–response curves obtained for the wild-type and L28R mutant strains (Figure 6A,B, respectively) clearly show that all compounds, except flavonic acid and oxyresveratrol, inhibit

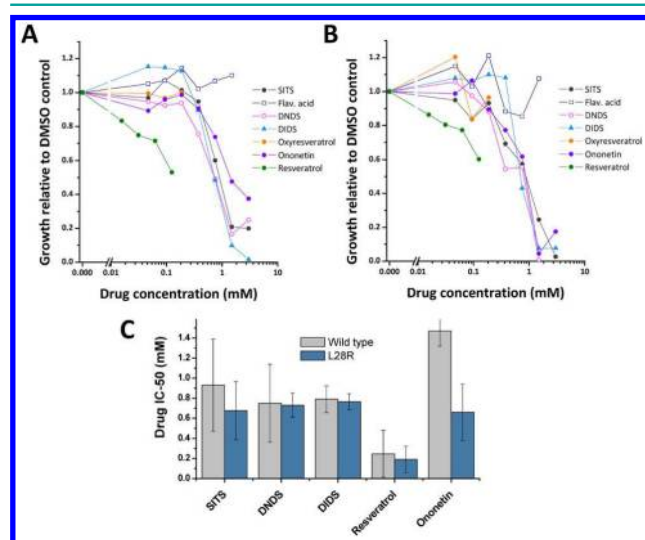


**Figure 6.** Growth inhibition of wild-type (A) and resistant (B) *E. coli* cells by deoxybenzoin and stilbenoid class of small molecules. Growth measurements were performed in duplicate for each drug concentration. (C)  $IC_{50}$  values determined from panels A and B by nonlinear curve fitting for each drug and for each *E. coli* strain.

growth of both strains within the range of concentrations tested. Moreover, in agreement with the enzymatic activity results obtained for the purified protein variants, the calculated *in vivo*  $IC_{50}$  values determined for the drug-resistant strain are also comparable to those obtained for the wild-type strain. Our results clearly point to an inhibition of DHFR activity targeted by these newly discovered small molecules as the cause for the arrest of bacterial growth.

It is important to note that resveratrol (the compound with highest inhibitory activity *in vivo*) had been previously reported to have antibacterial activity,<sup>29,30</sup> with an estimated  $IC_{50}$  of 0.25 mM, very similar to that determined in this work, although its mechanism of action has not been elucidated. To address if this molecule affects growth by specifically inhibiting DHFR, we tested the effect of resveratrol on *E. coli* cultures grown in media supplemented with a metabolic complement ( $folA_{mix}$ ) that is known to restore growth of cells treated with trimethoprim,<sup>31</sup> a potent, specific inhibitor of DHFR. The presence of  $folA_{mix}$  fully restores growth of cells inhibited by different resveratrol concentrations (Figure S9), indicating that this compound specifically blocks folate metabolism. This work provides the first evidence for the intracellular targeting of DHFR by this compound as one potential basis for the antibacterial activity demonstrated by this compound. Interestingly, introduction of an additional hydroxyl group to resveratrol seems to render this molecule biologically inactive, possibly due to differences in cell permeation properties.

## DISCUSSION

Previous analysis of drug–protein interactions and the demonstration of the limited number of geometrically distinct pockets on protein surfaces have implied that structurally diverse and distinct small molecules can bind to similar receptors.<sup>2</sup> However, all instances of diverse small molecules binding to a given protein of interest have relied extensively on serendipitous findings, and there are merely a handful of successful discoveries.<sup>32</sup> Moreover, the new small molecules are always minor alterations on the initial scaffolds thus expanding the novelty aspect incrementally.<sup>33</sup> This necessitates the development of tools that can search for novel scaffolds in a more systematic manner. In the current work, we demonstrate that a virtual ligand-screening algorithm that relies extensively on pocket similarity and ligand pruning,<sup>25</sup> when combined with chemically intuitive scaffold hopping, can yield interesting leads in terms of completely novel scaffolds that have the potential to bind and inhibit a medically important receptor protein.

All of the scaffolds described in the present work as inhibitors of DHFR, namely, stilbenoid, deoxybenzoin, and chalcones, have no precedence whatsoever in either binding or inhibiting DHFR. Further, given that a substantial number of them like resveratrol, oxyresveratrol, and ononetin are found in natural products like wine and legumes,<sup>34,35</sup> future exploration of them as potential therapeutic agents makes cytotoxicity on human cells less of a concern, making them valuable lead molecules. It has not escaped our attention that stilbenoids, like resveratrol, have been shown to possess anticancer activity with roles in modulating various pathways. However, none of these studies have ever indicated purine metabolism as a potential target and DHFR as the receptor that also gets modulated.<sup>34,36</sup> We, as an extension of our results, posit that, among other targets, resveratrol may bring about its anticancer activity by targeting purine metabolism through inhibiting human DHFR in cancer cells. This is the subject of a potentially interesting future study.

This study is an important attempt in translational research. Starting from computational attempts at predicting small-molecular binders, it validated the predicted binding and assessed inhibition of the intended target. Furthermore, it demonstrated differential inhibition across the wild-type and drug-resistant variants of the target protein and concluded by showing cytotoxic effects on *E. coli* harboring both wild-type and a drug-resistant rescue variant of the mutant enzyme.

Future extensions of this work will include improvement of activity and cell penetrability of the lead compounds to bring them into a viable therapeutic range as potential stand-alone drugs or components of natural-product formulations.

In conclusion, this is the first study that demonstrates the successful application of a pocket and ligand similarity based VLS algorithm to arrive at novel scaffolds and to employ systematic scaffold hopping to expand the small-molecule diversity space in inhibitor discovery. Ten molecules with ability to inhibit the drug-resistant variant of *EcDHFR* have been discovered and characterized. These molecules inhibit the protein by displaying a unique mechanism of inhibition and by binding to a novel site on the enzyme.

## METHODS

**Reagents.** All reagents and chemicals were of high quality and were procured from Sigma-Aldrich Co., USA, Amresco, or Fisher Scientific. Developmental Therapeutics Program (DTP) of the National Cancer Institute (NCI) provided a substantial fraction of the various small molecules employed in this study, while the rest were obtained from Sigma (Table S1).

**Wild-type and Mutant Protein Expression and Purification.** Wild-type and mutant proteins were expressed and purified as previously described.<sup>8</sup>

**Binding Studies Using DSF.** Binding of the molecules to *EcDHFR* was tested by DSF. The experiments were carried out following previously reported protocols from our lab.<sup>11,23</sup> Briefly, the reactions were carried out in 96 well plates on the RealPlex quantitative-PCR instrument (Eppendorf). The reaction mixture contained 100 mM HEPES, pH 7.3, and 150 mM NaCl with 5× concentration of Sypro orange. Various compounds were tested for binding at a final concentration of 500 μM with 5 μM of *EcDHFR*.

**Dihydrofolate Reductase Assay.** DHFR was assayed as previously reported.<sup>16</sup> Briefly, the conversion of NADPH was monitored as a decrease in absorbance at 340 nm for 100 s. The amount of product formed was computed using a molar-extinction coefficient ( $\epsilon$ ) of  $6.2 \times 10^3 \text{ M}^{-1} \text{ cm}^{-1}$  for  $\beta$ -NADPH at 340 nm.<sup>37</sup> The nonenzymatic hydrolysis of NADPH was normalized. Assays were initiated with enzyme, and the initial velocities, where product formation was less than 5%, were measured for reaction mixtures containing 100 mM HEPES, pH 7.3, at ~22 °C.

All the measurements were performed in duplicate, and the error values indicated are standard errors (SE). *EcDHFR* concentration was 16.7 nM.<sup>16</sup> All the data were fit using the nonlinear curve-fitting subroutines of GraphPad Prism, version 4.0 (GraphPad Software, Inc.).

**Inhibition Kinetics.** IC<sub>50</sub> determination assays were carried out in 100 mM HEPES, pH 7.3, 60 μM NADPH, 50 μM H<sub>2</sub>F, and variable concentration of each inhibitor. The enzyme concentration was as specified above. The curves were fit to eq 1,

$$y = 100\% / [1 + (I/IC_{50})] \quad (1)$$

where  $I$  is the inhibitor concentration and  $y$  is the percentage of activity.

Experimental  $K_i$  values were determined by titrating the substrates H<sub>2</sub>F and NADPH, around their respective  $K_m$  values, at various fixed concentrations of the inhibitors around their  $K_{i,app}$  values. The resulting substrate concentration versus velocity curves were fit to models of competitive inhibition (eq 2), noncompetitive inhibition (eq

3), uncompetitive inhibition (eq 4), and mixed-type inhibition (eq 5) in order to discriminate among the different types of inhibition and to estimate the various inhibition constants ( $K_i$ ).

Competitive:

$$v = V_{max}[S] / \{K_m(1 + [I]/K_i) + [S]\} \quad (2)$$

Noncompetitive:

$$v = V_{max}[S] / \{K_m(1 + [I]/K_i) + [S](1 + [I]/K_i)\} \quad (3)$$

Uncompetitive:

$$v = V_{max}[S] / \{K_m + [S](1 + [I]/K_i)\} \quad (4)$$

Linear Mixed-type:

$$v = V_{max,app}[S] / (K_{m,app} + [S])$$

$$V_{max,app} = V_{max} / (1 + [I]/(\alpha K_i))$$

$$K_{m,app} = K_m(1 + [I]/K_i) / (1 + [I]/(\alpha K_i)) \quad (5)$$

where  $v$  is the velocity of the reaction,  $V_{max}$  is the maximum velocity,  $[S]$  is the substrate concentration,  $[I]$  is the inhibitor concentration,  $K_m$  is the Michaelis–Menten constant, and  $K_i$  is the inhibition constant. Visual assessment of the type of inhibition was done with Lineweaver–Burk plots.

Plots showing substrate-inhibition behavior were fit using the following equation

$$v = V_{max}[S] / (K_m + [S] + [S]^2/K_i) \quad (6)$$

The double-reciprocal plot for the substrate inhibition was fit to the equation

$$1/v = K_m/V_{max} \times 1/[S] + 1/V_{max} + [S]/(V_{max}K_i) \quad (7)$$

In eq 7,  $[S]$  appearing in the denominator is the substrate for the enzyme, while  $[S]$  appearing in the numerator is the inhibitor, and hence, the double reciprocal plot shows upward curvature at high substrate concentrations.

**Computational Approach to Binding Site Prediction.** We used nine experimentally solved crystal structures<sup>38</sup> of *EcDHFR* (PDB IDs 1RX1, 1RX2, 1RX3, 1RX4, 1RX5, 1RX6, 1RX7, 1RX8, and 1RX9) to detect geometrical pockets (cavities) using the CAVITATOR<sup>39</sup> pocket-detection algorithm. CAVITATOR uses a grid-based method to assign residues to a pocket while excluding the ledge associated residues. The consensus residue pockets were defined as those detected in more than 75% of the structures. Next, using APoc,<sup>39,40</sup> we compared the predicted pockets of DHFR to the holo pockets of the HOLO-PDB template used in our previous study.<sup>41</sup> The library of holo-structures includes cocrystallized structures of protein–ligand complexes in which the ligand has at least six heavy atoms. The binding site is defined by considering protein residues with heavy-atom contacts with the ligand (distance less than 4.5 Å). Finally, the results were sorted using the pocket-similarity score, and their relevant statistical  $p$ -values were reported by APoc.

**Antibacterial Activity Assay.** The *E. coli* strain in which chromosomal *folA* gene had been replaced by mutant L28R was a kind gift from Dr. Roy Kishony. Prior to growth measurements, cells were grown overnight in minimal M9 medium at 30 °C. The following day, the cultures were used to inoculate a 384 well plate with M9 medium supplemented with different concentrations of drug (up to 3 mM) or the corresponding volume of DMSO alone. Resveratrol and oxyresveratrol could not be tested above 0.25 mM due to insolubility. The starting optical density was 0.005, and the growth measurements were performed at 30 °C using a Tecan Infinite M200 Pro plate reader. The ability of cells to grow at each drug concentration was assessed by computing the area under the growth curve (OD<sub>600nm</sub>) over a period of 15 h. Since the solvent (DMSO) itself showed inhibitory effects on growth (down to approximately 30% at the highest DMSO concentration used), the extent of inhibition at each

drug concentration was normalized against reference growth curves obtained in the presence of matching amounts of DMSO alone. Duplicate measurements were performed for each drug concentration. Rescue of growth by the mixture folA<sub>mix</sub> was tested by supplementing M9 media with 20 mg/L adenine, 80 mg/mL inosine, 200 mg/L thymine, 20 mg/L methionine, and 20 mg/L glycine.

## ■ ASSOCIATED CONTENT

### ● Supporting Information

The Supporting Information is available free of charge on the ACS Publications website at DOI: 10.1021/acschembio.7b00175.

Methods and results for ononetin–substrate interaction and DLS, SAR for chalcones (Figure S1), DLS (Figure S2), atypical inhibition by ononetin (Figure S3), wavelength spectra to assess substrate–cofactor–inhibitor interactions (Figure S4), inhibition by stilbenes (Figure S5), inhibition of wt and mutant *EcDHFR* by classical inhibitors (Figure S6), *EcDHFR* and its alternate pockets (Figure S7), predicted binding site for ononetin-like molecules (Figure S8), growth rescue of *E. coli* treated with resveratrol by metabolic complementation (Figure S9), compound list (Table S1), description of new pockets (Table S2), and alignment of *EcDHFR*'s PKT4 and binding site of bromo-resveratrol in hSirt3 (Table S3) (PDF)

## ■ AUTHOR INFORMATION

### Corresponding Author

\*E-mail: skolnick@gatech.edu. Tel: (404) 407-8975. Fax: (404) 385-7478.

### ORCID

João V. Rodrigues: 0000-0002-5605-656X

Jeffrey Skolnick: 0000-0002-1877-4958

### Notes

The authors declare no competing financial interest.

## ■ ACKNOWLEDGMENTS

This project was funded by 1R35GM118039 of the Division of General Medical Sciences of the NIH. We would also like to thank the Developmental Therapeutics Program of the National Cancer Institute for providing the small molecules used in this study.

## ■ ABBREVIATIONS

*EcDHFR*, *Escherichia coli* dihydrofolate reductase; NADPH, nicotinamide adenine dinucleotide phosphate, reduced; H<sub>2</sub>F, dihydrofolate; H<sub>4</sub>F, tetrahydrofolate; SAR, structure–activity relationship; HEPES, 4-(2-hydroxyethyl)piperazine-1-ethanesulfonic acid; HPPD, 4-hydroxyphenylpyruvate dioxygenase; SITS, 4-acetamido-4'-isothiocyano-2,2'-disulfonic stilbene; DIDS, 4,4'-diisothiocyano-2,2'-disulfonic stilbene; DNDS, 4,4'-dinitrostilbene-2,2'-disulfonate

## ■ REFERENCES

- (1) Panjkovich, A., and Daura, X. (2010) Assessing the structural conservation of protein pockets to study functional and allosteric sites: implications for drug discovery. *BMC Struct. Biol.* 10, 9.
- (2) Skolnick, J., and Gao, M. (2013) Interplay of physics and evolution in the likely origin of protein biochemical function. *Proc. Natl. Acad. Sci. U. S. A.* 110, 9344–9349.
- (3) Skolnick, J., Gao, M., Roy, A., Srinivasan, B., and Zhou, H. (2015) Implications of the small number of distinct ligand binding pockets in proteins for drug discovery, evolution and biochemical function. *Bioorg. Med. Chem. Lett.* 25, 1163–1170.
- (4) Schweitzer, B. I., Dicker, A. P., and Bertino, J. R. (1990) Dihydrofolate reductase as a therapeutic target. *FASEB J.* 4, 2441–2452.
- (5) McGuire, J. J. (2003) Anticancer antifolates: current status and future directions. *Curr. Pharm. Des.* 9, 2593–2613.
- (6) Watson, M., Liu, J. W., and Ollis, D. (2007) Directed evolution of trimethoprim resistance in *Escherichia coli*. *FEBS J.* 274, 2661–2671.
- (7) Toprak, E., Veres, A., Michel, J. B., Chait, R., Hartl, D. L., and Kishony, R. (2011) Evolutionary paths to antibiotic resistance under dynamically sustained drug selection. *Nat. Genet.* 44, 101–105.
- (8) Rodrigues, J. V., Bershtein, S., Li, A., Lozovsky, E. R., Hartl, D. L., and Shakhnovich, E. I. (2016) Biophysical principles predict fitness landscapes of drug resistance. *Proc. Natl. Acad. Sci. U. S. A.* 113, E1470–1478.
- (9) Stone, S. R., Morrison, J. F., and Mark, A. (1984) Interaction of analogues of nicotinamide adenine dinucleotide phosphate with dihydrofolate reductase from *Escherichia coli*. *Biochemistry* 23, 4340.
- (10) Kompis, I. M., Islam, K., and Then, R. L. (2005) DNA and RNA synthesis: antifolates. *Chem. Rev.* 105, 593–620.
- (11) Srinivasan, B., Zhou, H., Kubanek, J., and Skolnick, J. (2014) Experimental validation of FINDSITE(comb) virtual ligand screening results for eight proteins yields novel nanomolar and micromolar binders. *J. Cheminf.* 6, 16.
- (12) Fukunaga, J. Y., Hansch, C., and Steller, E. E. (1976) Inhibition of dihydrofolate reductase. Structure-activity correlations of quinazolines. *J. Med. Chem.* 19, 605–611.
- (13) Kuyper, L. F., Baccanari, D. P., Jones, M. L., Hunter, R. N., Tansik, R. L., Joyner, S. S., Boytos, C. M., Rudolph, S. K., Knick, V., Wilson, H. R., Caddell, J. M., Friedman, H. S., Comley, J. C., and Stables, J. N. (1996) High-affinity inhibitors of dihydrofolate reductase: antimicrobial and anticancer activities of 7,8-dialkyl-1,3-diaminopyrrolo[3,2-f]quinazolines with small molecular size. *J. Med. Chem.* 39, 892–903.
- (14) Rosowsky, A., Hynes, J. B., and Queener, S. F. (1995) Structure-activity and structure-selectivity studies on diaminoquinazolines and other inhibitors of *Pneumocystis carinii* and *Toxoplasma gondii* dihydrofolate reductase. *Antimicrob. Agents Chemother.* 39, 79–86.
- (15) Srinivasan, B., Skolnick, J., and Zhou, H. (2014) Molecules with potent DHFR binding affinity and antibacterial activity. US Patent 20140329840, Georgia Tech Research Corporation, United States.
- (16) Srinivasan, B., and Skolnick, J. (2015) Insights into the slow-onset tight-binding inhibition of *Escherichia coli* dihydrofolate reductase: detailed mechanistic characterization of pyrrolo [3,2-f] quinazoline-1,3-diamine and its derivatives as novel tight-binding inhibitors. *FEBS J.* 282, 1922–1938.
- (17) Baccanari, D. P., Daluge, S., and King, R. W. (1982) Inhibition of dihydrofolate reductase: effect of reduced nicotinamide adenine dinucleotide phosphate on the selectivity and affinity of diamino-benzylpyrimidines. *Biochemistry* 21, 5068–5075.
- (18) Chio, L. C., and Queener, S. F. (1993) Identification of highly potent and selective inhibitors of *Toxoplasma gondii* dihydrofolate reductase. *Antimicrob. Agents Chemother.* 37, 1914–1923.
- (19) Li, R. L., and Poe, M. (1988) Quantitative structure-activity relationships for the inhibition of *Escherichia coli* dihydrofolate reductase by 5-(substituted benzyl)-2,4-diaminopyrimidines. *J. Med. Chem.* 31, 366–370.
- (20) Hansch, C., Li, R., Blaney, J. M., and Langridge, R. (1982) Comparison of the inhibition of *Escherichia coli* and *Lactobacillus casei* dihydrofolate reductase by 2,4-diamino-5-(substituted-benzyl)-pyrimidines: quantitative structure-activity relationships, X-ray crystallography, and computer graphics in structure-activity analysis. *J. Med. Chem.* 25, 777–784.
- (21) Williams, J. W., Morrison, J. F., and Duggleby, R. G. (1979) Methotrexate, a high-affinity pseudosubstrate of dihydrofolate reductase. *Biochemistry* 18, 2567–2573.

- (22) Blaney, J. M., Hansch, C., Silipo, C., and Vittoria, A. (1984) Structure-Activity Relationships of Dihydrofolate Reductase Inhibitors. *Chem. Rev.* *84*, 333–407.
- (23) Srinivasan, B., Tonddast-Navaei, S., and Skolnick, J. (2015) Ligand binding studies, preliminary structure-activity relationship and detailed mechanistic characterization of 1-phenyl-6,6-dimethyl-1,3,5-triazine-2,4-diamine derivatives as inhibitors of *Escherichia coli* dihydrofolate reductase. *Eur. J. Med. Chem.* *103*, 600–614.
- (24) Lynch, C., Pearce, R., Pota, H., Cox, J., Abeku, T. A., Rwakimari, J., Naidoo, I., Tibenderana, J., and Roper, C. (2008) Emergence of a dhfr mutation conferring high-level drug resistance in *Plasmodium falciparum* populations from southwest Uganda. *J. Infect. Dis.* *197*, 1598–1604.
- (25) Roy, A., Srinivasan, B., and Skolnick, J. (2015) PoLi: A Virtual Screening Pipeline Based on Template Pocket and Ligand Similarity. *J. Chem. Inf. Model.* *55*, 1757–1770.
- (26) Nguyen, G. T., Gertz, M., and Steegborn, C. (2013) Crystal structures of Sirt3 complexes with 4'-bromo-resveratrol reveal binding sites and inhibition mechanism. *Chem. Biol.* *20*, 1375–1385.
- (27) Stierand, K., and Rarey, M. (2010) Drawing the PDB: Protein-Ligand Complexes in Two Dimensions. *ACS Med. Chem. Lett.* *1*, 540–545.
- (28) Palmer, A. C., Toprak, E., Baym, M., Kim, S., Veres, A., Bershtein, S., and Kishony, R. (2015) Delayed commitment to evolutionary fate in antibiotic resistance fitness landscapes. *Nat. Commun.* *6*, 7385.
- (29) Hwang, D., and Lim, Y. H. (2015) Resveratrol antibacterial activity against *Escherichia coli* is mediated by Z-ring formation inhibition via suppression of FtsZ expression. *Sci. Rep.* *5*, 10029.
- (30) Seukep, J. A., Sandjo, L. P., Ngadjui, B. T., and Kuete, V. (2016) Antibacterial and antibiotic-resistance modifying activity of the extracts and compounds from *Nauclea pobeguini* against Gram-negative multi-drug resistant phenotypes. *BMC Complementary Altern. Med.* *16*, 193.
- (31) Kwon, Y. K., Higgins, M. B., and Rabinowitz, J. D. (2010) Antifolate-induced depletion of intracellular glycine and purines inhibits thymineless death in *E. coli*. *ACS Chem. Biol.* *5*, 787–795.
- (32) Bohm, H. J., Flohr, A., and Stahl, M. (2004) Scaffold hopping. *Drug Discovery Today: Technol.* *1*, 217–224.
- (33) Sun, H., Tawa, G., and Wallqvist, A. (2012) Classification of scaffold-hopping approaches. *Drug Discovery Today* *17*, 310–324.
- (34) Jang, M., Cai, L., Udeani, G. O., Slowing, K. V., Thomas, C. F., Beecher, C. W., Fong, H. H., Farnsworth, N. R., Kinghorn, A. D., Mehta, R. G., Moon, R. C., and Pezzuto, J. M. (1997) Cancer chemopreventive activity of resveratrol, a natural product derived from grapes. *Science* *275*, 218–220.
- (35) Straub, I., Mohr, F., Stab, J., Konrad, M., Philipp, S. E., Oberwinkler, J., and Schaefer, M. (2013) Citrus fruit and fabacea secondary metabolites potently and selectively block TRPM3. *Br. J. Pharmacol.* *168*, 1835–1850.
- (36) Signorelli, P., and Ghidoni, R. (2005) Resveratrol as an anticancer nutrient: molecular basis, open questions and promises. *J. Nutr. Biochem.* *16*, 449–466.
- (37) Horecker, B. L., and Kornberg, A. (1948) The extinction coefficients of the reduced band of pyridine nucleotides. *J. Biol. Chem.* *175*, 385–390.
- (38) Sawaya, M. R., and Kraut, J. (1997) Loop and subdomain movements in the mechanism of *Escherichia coli* dihydrofolate reductase: crystallographic evidence. *Biochemistry* *36*, 586–603.
- (39) Gao, M., and Skolnick, J. (2013) APoc: large-scale identification of similar protein pockets. *Bioinformatics* *29*, 597–604.
- (40) Gao, M., and Skolnick, J. (2013) A comprehensive survey of small-molecule binding pockets in proteins. *PLoS Comput. Biol.* *9*, e1003302.
- (41) Tonddast-Navaei, S., Srinivasan, B., and Skolnick, J. (2017) On the importance of composite protein multiple ligand interactions in protein pockets. *J. Comput. Chem.* *38*, 1252–1259.